Petroleum Science 21 (2024) 2169–2183

Contents lists available at ScienceDirect

Petroleum Science

journal homepage: www.keaipublishing.com/en/journals/petroleum-science

Review Paper

Research progress on micro-force measurement of a hydrate particle system

Qiang Luo [a], Wei Li [a], Zhi-Hui Liu [a], Feng Wang [b], Zhi-Chao Liu [a], Fu-Long Ning [a, *]

[a] Faculty of Engineering, China University of Geosciences (Wuhan), Wuhan, 430074, Hubei, China
[b] Suzhou Laboratory, Suzhou, 215000, Jiangsu, China

ARTICLE INFO

Article history:
Received 9 October 2023
Received in revised form
19 January 2024
Accepted 20 March 2024
Available online 28 March 2024

Edited by Jie Hao and Meng-Jiao Zhou

Keywords:
Clathrate hydrates
Hydrate particle
Micro-force measurements
Adhesion
Interactions

ABSTRACT

It remains a great challenge to understand the hydrates involved in phenomena in practical oil and gas systems. The adhesion forces between hydrate particles, between hydrate particles and pipe walls, and between hydrate particles and reservoir particles are essential factors that control the behaviors of clathrate hydrates in different applications. In this review, we summarize the typical micro-force measurement apparatus and methods utilized to study hydrate particle systems. In addition, the adhesion test results, the related understandings, and the applied numerical calculation models are systematically discussed.

1. Introduction

Natural gas hydrates are solid, non-stoichiometric compounds composed of small gas molecules and water under high-pressure and low-temperature conditions (Sloan, 2003) and are commonly known as combustible ice. In 1811, Humphrey Davy accidently discovered the first known gas hydrate, a crystalline compound formed by chlorine and water, in an experiment (Koh et al., 2011). In the early twentieth century, Hammerschmidt's observations revealed that another possibility of blockage in a natural gas pipeline resulted from the massive formation of natural gas hydrates inside (Hammerschmidt, 1934). With increasing concerns on issues including energy shortages, global warming, and environmental pollution, natural gas hydrates, which are a clean non-conventional energy source, have received more attention (Ning et al., 2012). From the middle of the twentieth century to the beginning of this century, hydrates were successively discovered in the Gulf of Mexico, the Nankai Trough, the Krishna-Godavari Sea area, the Yuling Basin, the South China Sea, and other places around the world (Li et al., 2016; Alberto, 2021). With support from the deep sea drilling program (DSDP), the ocean drilling program (ODP), the integrated ocean drilling Program (IODP), and other projects, comprehensive exploration of natural gas hydrate resources has been carried out, and the distribution of natural gas hydrates on a global scale has been gradually ascertained (Sloan, 2007; Collett et al., 2014). Since the beginning of this century, Canada, the United States, Japan, and China have carried out gas hydrate production tests in Mackenzie, the Alaska North Slope, the Nankai Trough, and the Shenhu area in the South China Sea, China carried out two rounds of production testing in the Shenhu area in 2017 and 2020, which achieved a leap from exploration to experimental production (Chen et al., 2020).

The exploration and production tests on natural gas hydrates have promoted studies of hydrate reservoir mechanics and sand control. Seismic inversion, logging, coring analysis, and in-situ cone penetration are the main methods for testing the mechanical properties of hydrate reservoir sediments (Wang et al., 2020a). In the laboratory, direct shear (Liu et al., 2017), triaxial shear (Song et al., 2010; Miyazaki et al., 2011; Hyodo et al., 2013; Yoneda et al., 2015; Zhang et al., 2015), acoustic wave (Winters et al., 2007), creep deformation (Durham et al., 2003), stretching (Jung et al., 2011), bending (Ohmura et al., 2002), and resonance column (Liu et al., 2020; Wang et al., 2020) have been tested to determine the mechanical properties of hydrate sediments and to

* Corresponding author.
E-mail address: nflzx@cug.edu.cn (F.-L. Ning).

https://doi.org/10.1016/j.petsci.2024.03.017

reveal the mechanical responses of hydrate sediments under different conditions. To study the microstructure of hydrates, novel techniques such as atomic force microscopy (Peng et al., 2019), X-ray computed tomography (X-CT) (Jin et al., 2006; Schindler et al., 2017; Seol et al., 2019), Raman spectroscopy (Guo et al., 2020), nuclear magnetic resonance (NMR) (Cha et al., 2015), cryogenic scanning electron microscopy (Stern et al., 2004), distributed optical fiber sensor (Teng et al., 2021), and in-situ neutron diffraction (Sloan, 2007) have been used to observe phenomena such as the distribution of hydrates in hydrate sediments, the pore structure, and fluid migration. With the development of micro-electronic mechanical systems, precision machining, micro-nano manipulation, and other technologies in recent decades, a large number of micro-force measurement apparatuses have been designed and built for the mechanical testing of small hydrate particles.

At present, micro-force measurements mainly involve the contact mechanics test between hydrate particles and the strength test of hydrate agglomerates, which are important for evaluating the performance of hydrate anti-aggregation agents (inhibitors) and hydrate reservoir strength criteria. Compared with macro-mechanical measurements, micro-force measurements can be used to directly study the microstructure and contact mechanical properties of hydrates and skeleton particle migration. From the microcosmic perspective, this fundamental research not only contributes to pipeline flow assurance and inhibitor evaluation but also benefits the study of mechanical behavior and the understanding of the sand production mechanism during hydrate reservoir exploitation. This article summarizes the existing typical micro-force measurement apparatuses and methods used to study hydrate particle systems, and the mechanical measurement values, the main understandings, and the applied numerical calculation models are discussed in detail. The goal of this review is to provide a reference for subsequent hydrate reservoir particle interaction testing and an overview of the basic research methods for solving the key scientific problems in the safe and efficient exploitation of hydrates.

2. Micro-force measurement apparatuses and methods

Apparatuses used for hydrate particle system measurement require temperature or pressure control components. In addition, the microscopic observation and force measurement components are required to have high accuracy. The methods of measuring the mechanical properties of microstructural materials mainly include the nano-indentation method, tympanic membrane method, resonance method, cantilever beam method, and micro-stretching method (Liu et al., 2008). By adopting micro-nano technology and micro-manipulation technology, a micro-force measurement apparatus uses a high-precision electric stage to control micro-nano movement and to conduct tension and compression measurements on hydrates formed under controlled temperature/pressure conditions. The apparatus can also achieve real-time image acquisition analysis of the movement process through the integration of high-resolution digital image acquisition instruments.

2.1. Cantilever beam method

2.1.1. Micromechanical force apparatus for hydrates

A typical apparatus for measuring the mechanical properties of a hydrate particle system is the micromechanical force (MMF) apparatus (Fig. 1), which mainly uses the cantilever beam method to calculate the force based on the deformation of the cantilever and the conversion of the elastic coefficient. The MMF apparatus has been utilized for nearly two decades, and a large number of measurements between hydrate particles have been conducted using it. Considerable experimental measurement data for hydrate particle mechanics comparison have been generated, and abundant theoretical analysis models have been established. The development of the MMF apparatus consisted of three phases. First, inspired by the work of Fan et al. (2003) on ice particle adhesion measurement, Yang et al. built an MMF apparatus that can measure the adhesion between tetrahydrofuran hydrate (THF(H)) particles under controlled temperature conditions (Yang et al., 2004). Subsequently, Taylor et al. (2007) improved Yang et al. (2004)'s work by installing a plexiglass chamber around the stage to reduce the impacts of humidity and condensed water, and they optimized the sample clamping and measurement operation process. In this phase, the components of the MMF apparatus include an optical microscope equipped with a digital camera, a micromanipulator, a glass fiber, a stage with a cooling liquid circulating jacket, and a circulating bath (Aman et al., 2013), and a large number of measurements were performed using the apparatus. Lee et al. took Yang et al. (2004) and Taylor et al. (2007)'s work one step further (Lee et al., 2014, 2015). They built a high-pressure micromechanical force apparatus (HP-MMF) (Fig. 1(b)–(c))), which can operate under high pressure (10 MPa), making mechanical measurement under high-pressure conditions possible. The HP-MMF includes a reactor for pressure control and integrates the main components of the atmospheric MMF into the pressure reactor.

The test environment of the MMF apparatus has been developed from the gas phase to the liquid phase and from atmospheric conditions to high-pressure conditions. The mechanical properties of the particles are calculated from the elastic deformation and considering the elastic parameters of the glass fiber probe. A typical measurement using the MMF apparatus includes the following steps (Fig. 2) (Aman et al., 2013): (1) the hydrate particle at one end of the vertical glass fiber is moved toward the top of the hydrate particle at the end of the horizontal glass fiber. (2) The vertical glass fiber is moved down, enabling two hydrate particles to come in contact with each other and achieving preloading (achieved by the step size ΔP). (3) After waiting for a certain period of time (contact time), the two particles are separated from each other using the upward pull force. (4) The image is captured by a high-speed camera, and ΔD is calculated using image analysis software. Then, ΔD is multiplied by the elastic constant of the glass fiber probe to obtain the adhesion force between the two particles (Aman et al., 2013; Hu et al., 2017).

2.1.2. Atomic force microscope for hydrate mechanical measurement

The atomic force microscope (AFM) has been widely applied in the study of the surface morphology, surface chemistry, and electrical, thermal, and magnetic properties of various materials at the micro-nano scale (Petrenko, 1997). Although the MMF apparatus was originally built using the working principle of the AFM, the application of the AFM for hydrate investigation occurred ten years later than the development of the MMF apparatus for hydrate systems. For the first time, Peng et al. used a modified cryogenic AFM (Fig. 3) to characterize THF(H) synthesized at different temperatures and on different interfaces, and they analyzed the effects of the temperature and contact interfaces on its surface characteristics (Peng et al., 2018). They measured the interactions between a silica (SiO_2) microsphere colloidal probe with a diameter of 5 μm and THF(H), as well as the interactions between the hydrate in simulated pores and the sediment framework (Peng et al., 2019). Under temperatures of −30 °C to −10 °C and probe driving rates of 0.5–20 μm/s, they investigated the influences of the depth of the microspheres pressed into the THF(H) sample, the contact time, and the contact force on the adhesion force between the microspheres and the THF(H) samples. The results indicate that the

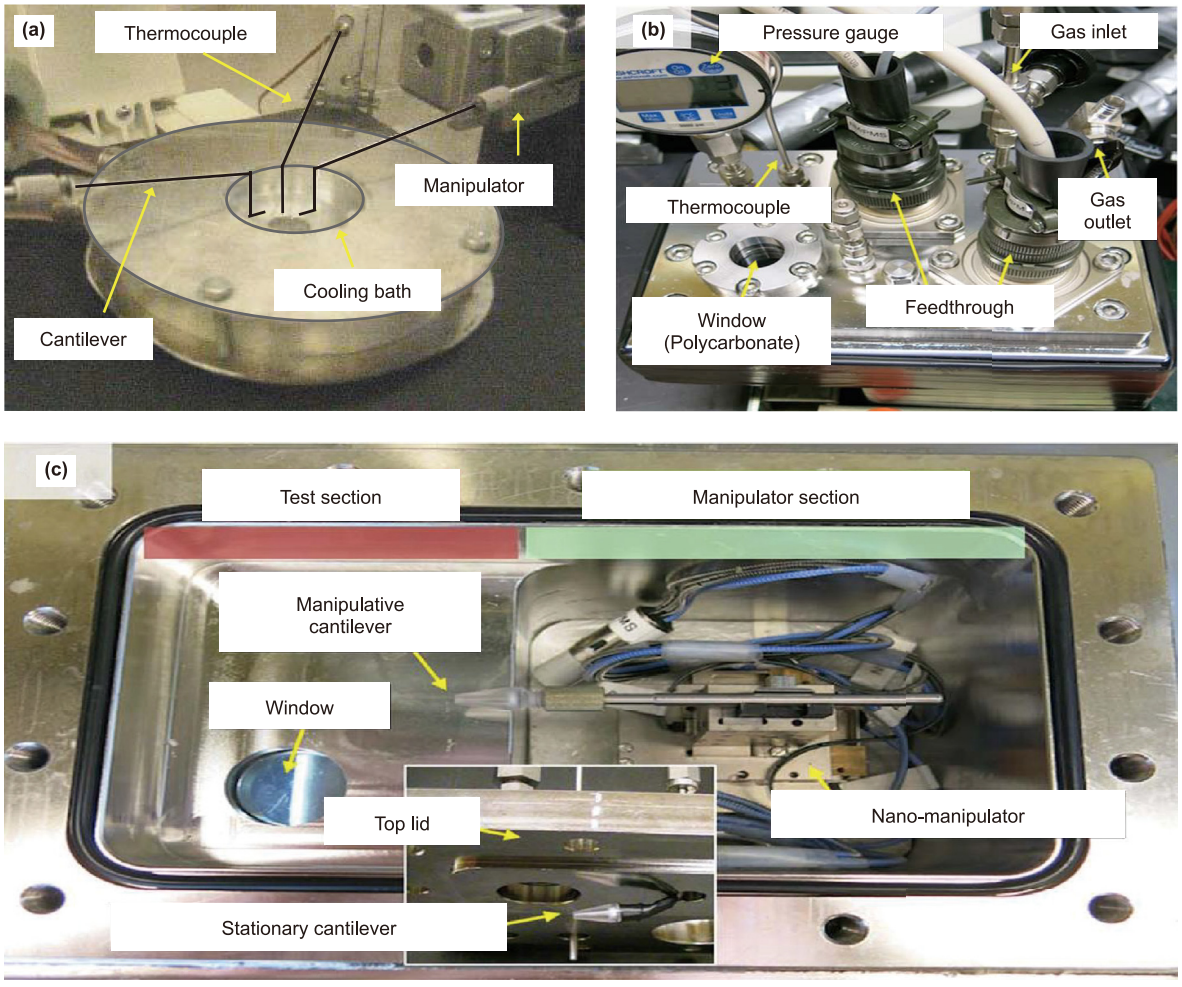

Fig. 1. **(a)** MMF of early loading plexiglass chamber (Taylor et al., 2007); **(b)** HP-MMF: external component; **(c)** HP-MMF: internal component (Lee et al., 2014, 2015).

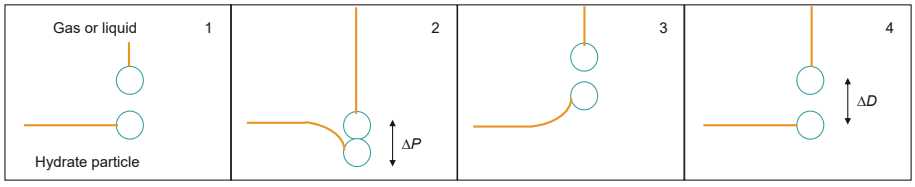

Fig. 2. MMF test steps (redrawn after Aman et al. (2012a) and Hu et al. (2017)).

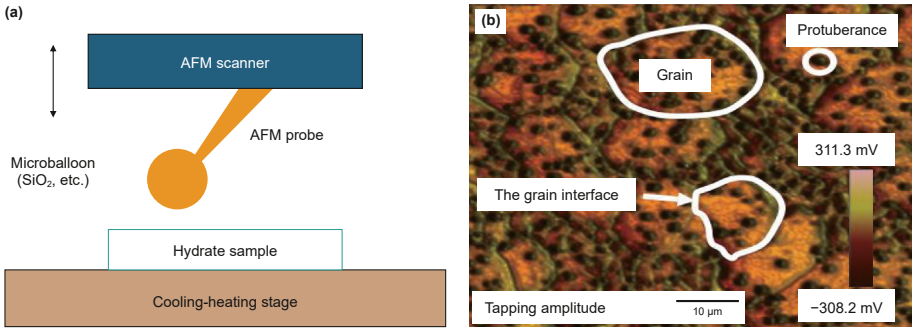

Fig. 3. Cryogenic AFM: **(a)** Schematic diagram of core components; **(b)** THF hydrate morphology from AFM (adapted from Peng et al. (2018)).

THF(H) underwent plastic deformation during the intrusion process, and the hydrate-phase transformation induced by the intrusion may have further enhanced the plastic behavior. Recently, Nguyen et al. also tested the cohesion between solid spheres and a tetrahydrofuran clathrate slab. The slab was 0.3 mm thick and had better transparency to allow probing of the contact area from the bottom up via microscopy (Nguyen et al., 2021). Based on the work of Peng et al., Li et al. studied the effect of surfactants on the surface of THF hydrate by using AFM (Li et al., 2023), and confirmed the existence of a quasi–liquid layer (QLL) on the surface of THF hydrate (Li et al., 2024). The cryogenic AFM can not only measure the force between the reservoir particles and hydrates but also perform nanoscale characterization of the surface morphology of hydrate samples, which contribute to research on the basic properties of hydrates at the nano-micro scale.

2.2. Micro-stretching method

The hydrate measurement apparatus using the micro-stretching method mainly applies high-precision electromagnetic drive motors, micro-spring mechanics sensors, and strain gauges to implement the micro-load, and it directly tests the forces in the process. Thus, the cumbersome deformation calculation process of the cantilever method can be avoided, and the force value test is stable and repeatable. The abovementioned mechanical testing tools are generally placed in a reactor with a temperature control function to perform tests under normal or high pressures.

2.2.1. Apparatus for measuring the contact force between hydrates and water droplets

Song et al. (Cha et al., 2013; Song et al., 2010; Song et al., 2010, 2010) used a tensiometer and an electric displacement platform to build an experimental device for directly measuring the contact force between cyclopentane hydrate (CP(H)) and water droplets (Fig. 4). The test was conducted in a reactor under temperature-controlled hydrocarbon conditions. The CP hydrate probe was slowly brought into contact with water to determine the initial contact force. The core components of the device are a high-precision microbalance (KSV film balance 2000, 0.1 μN) and a motorized stage that moves in the vertical direction. They can achieve a repeatable initial contact force between the hydrate and water droplets.

2.2.2. Apparatus for measuring micro-strength of hydrate

Jung et al. (2011) developed a micro-strength measurement apparatus composed of strain gauges in a high-pressure cell (Fig. 5). They measured the bonding and peel strengths by applying external tension to hydrates with different guest molecules (CO_2, CH_4, THF, and ice) formed between a mica and calcite matrix. Their results revealed that the CO_2 hydrate and CH_4 hydrate underwent tensile failure when calcite was used as the base, while the ice and all of the other hydrates exhibited adhesion failure on the mica. When the failure occurs in the hydrate sample, it represents the tensile strength of the hydrate, and when the failure occurs at the interface between the hydrate and substrate, it represents the adhesion strength (Fig. 5(b)–(c)). The apparatus can simulate the tensile strengths of different hydrates and the adhesion strengths between different minerals and hydrates in a controllable environment.

2.2.3. Experimental apparatus for measuring the cohesion of methane hydrate

Sato et al. (2016) arranged a force sensor in a cell (Fig. 6) and tested the tensile strength of the methane hydrate (CH_4(H)) sample formed. The CH_4(H) powder was molded in the sample holder, and the sample holder was set in a pressure cell to guarantee that the contact area was sufficient. The inside of the cell was filled with dry methane gas or water, and the temperature and pressure were adjusted using a cooling pool and an injection pump, respectively (Sato et al., 2016). Under a constant pressure, the temperature, contact force, and contact time can be adjusted in the experiments. The most important feature of this apparatus is the optimization of the sample formation and the clamping method, which guarantee sufficient contact area between the tested samples. Therefore, compared with the MMF apparatus, this set up produces more repeatable strength data.

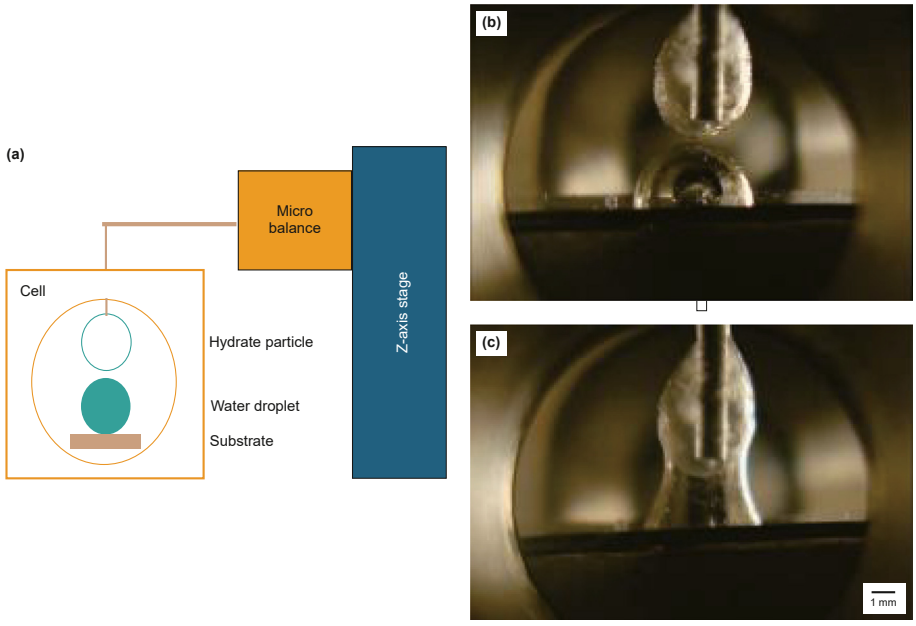

Fig. 4. The initial contact force test apparatus: **(a)** Schematic diagram of core components; **(b)** hydrate sample and water droplets in contact; **(c)** being pulled apart (adapted from Song et al. (2010) and Cha et al. (2013)).

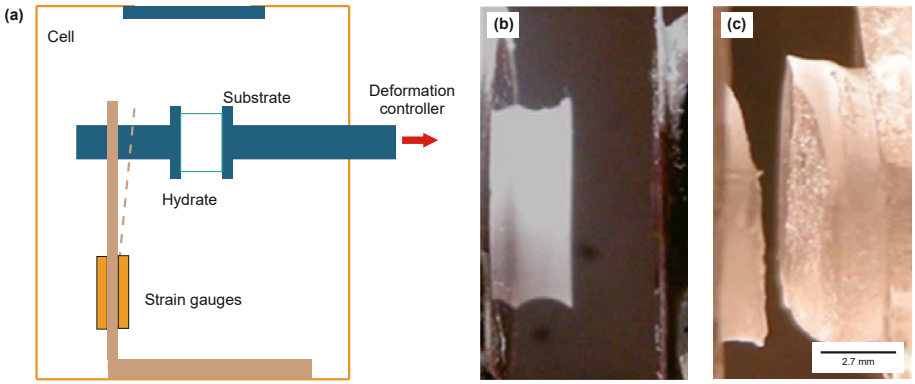

Fig. 5. The micro-strength measurement apparatus for hydrates: **(a)** Schematic diagram of core components; **(b)** sample failure occurs at the surface of the substrate; **(c)** failure occurs in the hydrate (adapted from Jung et al. (2011)).

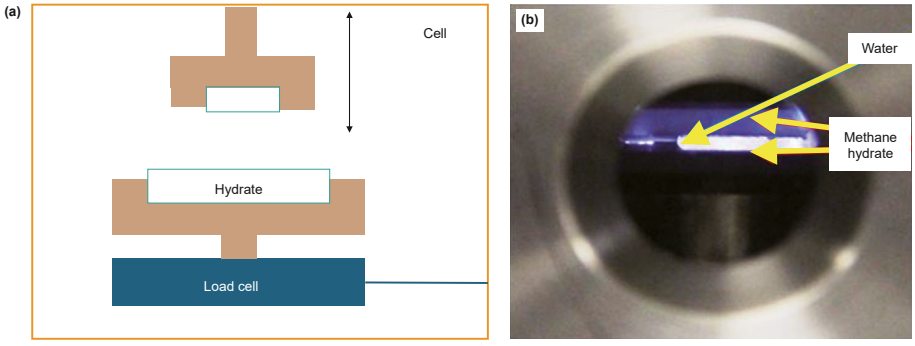

Fig. 6. The micro-cohesion strength measurement apparatus for CH_4(H): **(a)** Schematic diagram of the core components; **(b)** material objects and samples (adapted from Sato et al. (2016)).

2.2.4. Apparatus for measuring micro-adhesion strength between hydrate and pipe wall

This apparatus uses a fixed dynamometer on a sliding table to perform adhesion failure tests on hydrates formed on different substrates (Fig. 7) (Liu et al., 2020; Smith et al., 2012; Sojoudi et al., 2015). The measurement system includes a hydrate layer formation unit, an adhesion strength measurement unit, a temperature control device, and a microscopic observation system, which is used to record the formation process and thickness of the hydrate layers (Liu et al., 2020a). This type of apparatus can be used to study the influences of factors such as the formation time, surface roughness, material type, and subcooling on the hydrate adhesion strength and provides a method for simulating the shear failure process of hydrates after adhering to the wall of a pipeline.

2.2.5. Apparatus for measuring interaction between particles in a hydrate reservoir

To promote microscopic understanding of the mechanical mechanism of hydrate reservoir instability and sand production behavior, Yu et al. (2021) developed a micro-force test apparatus that can measure the force between reservoir particles (Fig. 8) and proposed a corresponding measurement method. Luo et al. (2022) used this device to study the tangential force between two THF(H) particles in the gas phase. The apparatus includes three programmable linear electric translation stages and two high-precision force sensors. One of the electric stages is used to realize horizontal movement in the *X* direction, and the other two electric stages are superimposed to realize linkage in the *Y* and *Z* directions. The positioning accuracy of the electric stage is 0.5 μm. The high-precision force sensor has a force measurement accuracy of 0.01 mN, and it can measure the tension force (positive value) and compression force (negative value) in real time. The friction between ice particles, THF(H) particles, and South China Sea sand particles has been measured using this apparatus. In addition, this apparatus can test the shear failure behavior between hydrate particles and sand particles or flat plates. This method simulates the

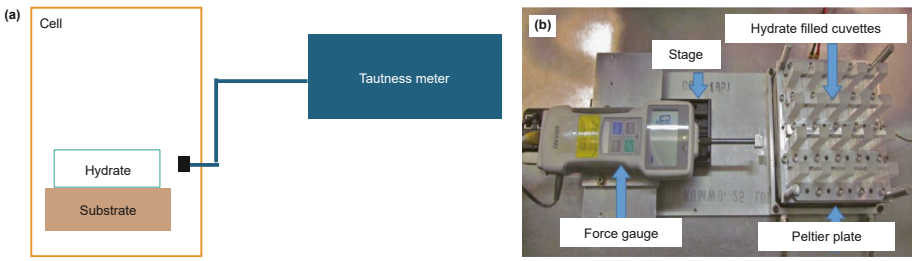

Fig. 7. The apparatus for measuring the micro-adhesion strength between a hydrate and a pipe wall: **(a)** Schematic diagram of the core components; **(b)** example of apparatus (adapted from Liu et al. (2020) and Smith et al. (2012)).

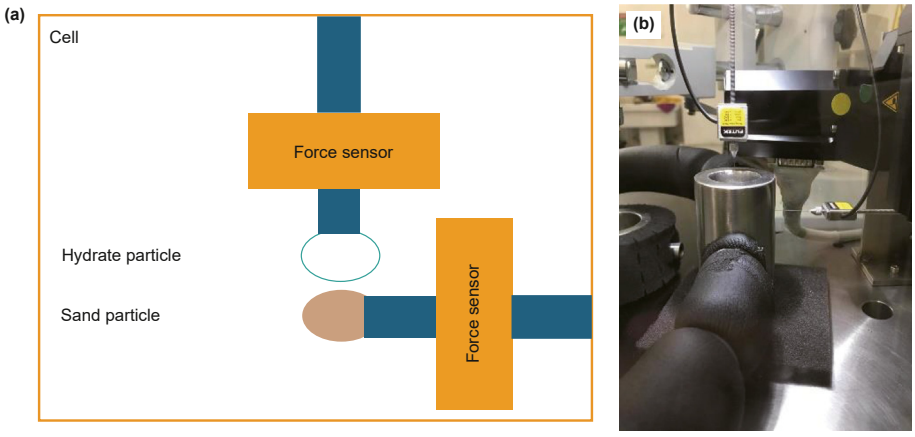

Fig. 8. The apparatus for measuring interaction between reservoir particles: **(a)** Schematic diagram of the core components; **(b)** material objects (adapted from Yu et al. (2021)).

shear failure process of hydrate particles in oil and gas pipelines, and it simulates and evaluates the reservoir instability and sand production caused by an intergranular shear failure among particles in the hydrate storage layer.

2.3. Other modified apparatuses

The abovementioned methods have played a vital role in understanding the formation of hydrate particles and in measuring the forces between particles. At present, various emerging physical and chemical microscopic testing methods have been introduced in hydrate research.

2.3.1. Quartz crystal microbalance for hydrate measurement

Lee et al. (2011) built a set of apparatus based on the quartz crystal microbalance (QCM) (Fig. 9) to measure the phase equilibrium and memory effect of hydrates. As the battery was gradually heated, the hydrate placed on the quartz crystal dissociated at a specific temperature and pressure (Lee et al., 2011). In addition, significant frequency and resistance changes were observed and occurred very quickly. At a fixed pressure, the dissociation temperature represents the thermodynamic equilibrium points of the liquid phase (water), gas phase, and hydrate phase. In the QCM method, data can be obtained at a rate of one equilibrium point per hour, which is about 30 times faster than the traditional temperature search method (Lee et al., 2011). The QCM with dissipation (QCM-D) takes the QCM technology one step further. A quartz crystal produces a resonance frequency under the action of an electric current, and the latest QCM-D has an additional shear vibration. When the current is turned off, the vibration attenuates, and this is recorded to obtain the resonance frequency (f) and dissipation factor (D) (Notley et al., 2005). Therefore, real-time interaction measurements between molecular layers, thickness and water content measurement, and parallel adhesion measurement can be carried out. These measurements are helpful in microscopic studies such as studies on the movement of guest molecules during hydrate formation, a liquid-like layer on the hydrate surface, and nano-level adhesion.

2.3.2. X-ray CT and three-axis combination for hydrates

Seol et al. (2019) proposed a novel measurement module that integrates a core holder and other specially designed experimental components with an X-ray CT scanner. This apparatus can perform pore-scale visualization and triaxial measurement to detect methane hydrate-bearing sediments in a controlled environment (Fig. 10). The characterization at the pore scale can be compared with the aforementioned hydrate measurements. The measurement module allows for temperature adjustment and independent control of four pressures: the inlet pressure, outlet pressure, confining pressure, and axial pressure. For a specimen with a diameter of 9.5 mm and a length of 19 mm, effective axial and transverse stresses can be applied separately, while the pore pressure and temperature are controlled to maintain the stability of the methane hydrate (Seol et al., 2019). The measurement module also includes an X-ray transparent beryllium core holder for 3-D computed tomography during triaxial loading. In addition to traditional stress-strain measurements, the test module allows the exploration of hydrate–sediment interactions at the pore scale, which demonstrates the application of the measurement module in estimating the geomechanical properties of methane hydrate-bearing sediments.

The main functions, accuracy and characteristics of the above typical hydrate particle system measuring instruments are as follows (Table 1).

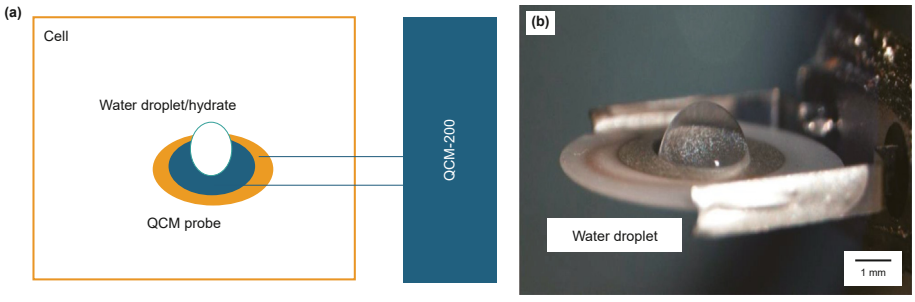

Fig. 9. The QCM measurement of the hydrate-phase equilibrium: **(a)** Schematic diagram of the core components; and **(b)** material objects (adapted from Lee et al. (2011)).

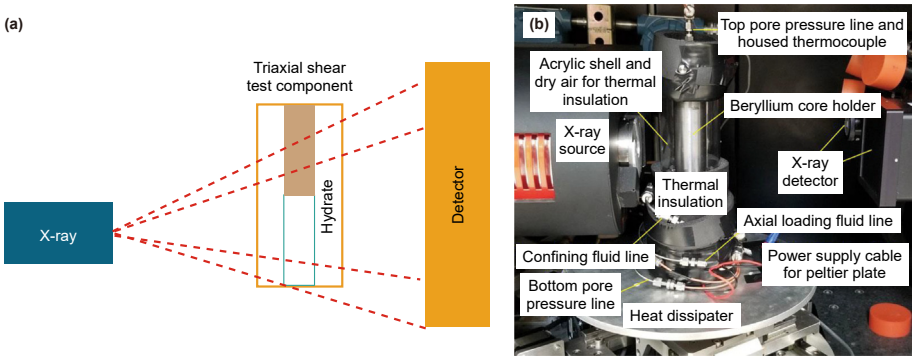

Fig. 10. X-CT combined with three-axis apparatus: **(a)** Schematic diagram of core components; **(b)** material objects (adapted from Seol et al. (2019)).

Table 1
Comparison list of test methods.

Test method		Applicability	Accuracy	Advantage	Recommendations for improvement
Cantilever beam method	*Micromechanical force apparatus for hydrates*	Force (adhesion; cohesive),	0.1 μN	Simple structure	Cannot be tested in real time; large amount of data processing
	Atomic force microscope for hydrate mechanical measurement	Force (adhesion; cohesive), surface topography.	1 pN	Nanometer scale; Atomic level.	Samples can only be stored at low temperatures during testing.
Micro-stretching method	*Apparatus for measuring the contact force between hydrates and water droplets*	Force (adhesion; cohesive)	0.1 μN	High accuracy; good repeatability.	Cannot be tested in a pressure environment.
	Apparatus for measuring micro-strength of hydrate	Tensile strength	kPa −MPa	Simple test method under pressure environments	No shear test function; large sample size
	Experimental apparatus for measuring the cohesion of methane hydrate	Tensile strength	kPa −MPa	Sample contact area quantification.	No shear test function; large sample size
	Apparatus for measuring micro-adhesion strength between hydrate and pipe wall	Shear strength	kPa −MPa	Simple shear test method	Cannot be tested in a pressure environment.
	Apparatus for measuring interaction between particles in a hydrate reservoir	Force (adhesion; cohesive; shear), friction coefficient.	0.01 mN	Both tensile and shear tests are available.	Cannot be tested in a pressure environment.
Other modified apparatuses	*Quartz crystal microbalance for hydrate measurement*	Resonance frequency; dissipation factor,	150 MHz	Molecular level.	Direct interaction between particles is not possible.
	X-ray CT and three-axis combination for hydrates	Strength	kPa −MPa	Pore scale visualization of triaxial shear testing.	Inadequately describe at the particle scale because of large sample sizes.

3. Micro-force measurement results for a hydrate particle system

With the development of micro-force measurement technology, the interparticle forces in various hydrate particle systems, including ice and THF(H), cyclopentane hydrate (CP(H)) and ethylene oxide hydrate (ETO(H)), carbon dioxide hydrate (CO_2(H)) and CH_4(H), and water droplets and different adhesion surfaces (Aman et al., 2014; Aspenes et al., 2010; Liu et al., 2023; Nicholas et al., 2009; Wang et al., 2017b; Luo et al., 2022) (e.g., stainless steel, carbon steel, glass, and aluminum), have been extensively investigated (Fig. 11)(Cha et al., 2013; Dieker et al., 2009; Hu et al., 2017; Liu et al., 2015, 2017; Peng et al., 2018; Song et al., 2010; Taylor et al., 2007). The mechanical performances have been measured under different contact conditions (e.g., contact time, contact force, and temperature), different gas-saturated environments (e.g., air, decane, nitrogen, CP, carbon dioxide, and methane), and different liquid-saturated environments (e.g., decane, CP, oil and surface activity, and water) (Aman et al., 2011, 2013; Aman et al., 2012a,b; Sato et al., 2016; Song et al., 2010; Luo et al., 2022). These measurements and evaluations provide valuable experimental insights for simulating hydrate blockage in oil pipelines.

3.1. Cohesion

The force required to pull apart two hydrate particles that are in contact is generally defined as the cohesive force between the hydrate particles, which reflects the tensile strength of the hydrate to some extent. At present, the cohesion measurement results for hydrate particles in the gas phase and liquid phase differ greatly. Specifically, the cohesion between hydrate particles in the gas phase is twice that in the oil phase and six times that in the water phase (Aman et al., 2012a,b). In the gas phase, humidity also affects the particle contact force (Rabinovich et al., 2002). The cohesion between hydrate particles measured in humid air (water saturation) is greater than that under dry air conditions (Aman et al., 2012a,b). Moreover, the cohesion between hydrate particles in the gas phase is linearly related to the effective radius of the particles, but it is unrelated to the particle size in the oil phase and water phase (Wang et al., 2020).

The cohesion in the gas phase is generally measured in an environment such as air, nitrogen, and hydrocarbon gases. In the gas-phase environment, the influences of humidity and other gas conditions are inevitable. The cohesion measured in humid air is larger than that under dry conditions and is generally higher than that in a liquid environment (Aman et al., 2011). These differences result from hydrate formation under experimental conditions and the rough surface morphology of hydrate particles (Aman et al., 2011). The rough surface creates more liquid bridges in the contact area, thereby increasing the cohesion value (Wang et al., 2020). Ice particles and THF(H) particles have similar adhesion behaviors, and the measured adhesion force shifts to a lower value as the temperature decreases from the melting point. The adhesion between CP hydrate particles under pressure is slightly higher than the value under normal pressure (Fig. 12). In addition, the NaCl

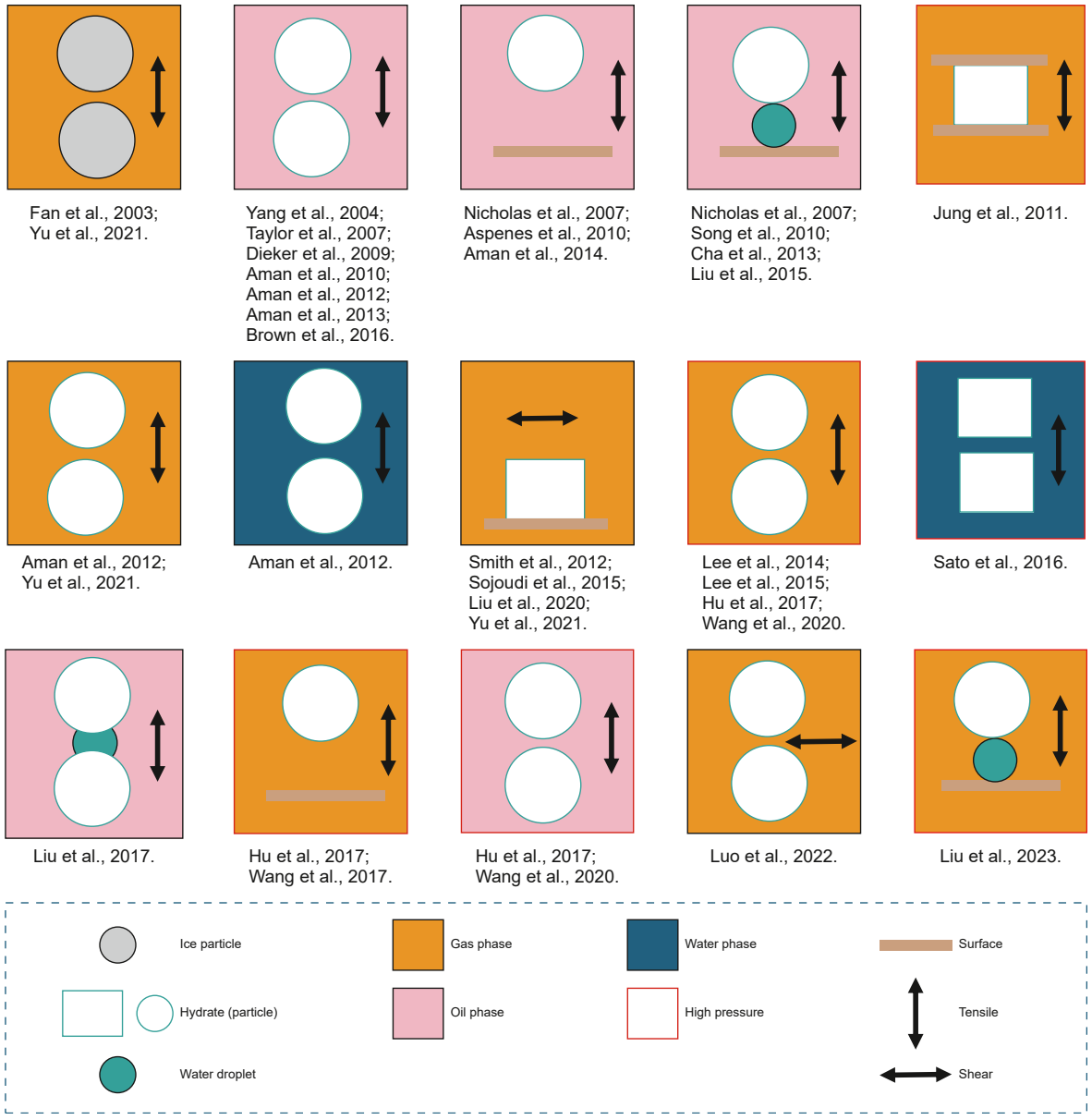

Fig. 11. Development of micro-force measurement of a hydrate particle system.

concentration of the liquid before hydrate particle formation has a significant effect on the cohesion between natural gas hydrate particles, and the cohesion significantly decreases as the NaCl content increases from 0 wt% to 5 wt%.

Under liquid-phase conditions, particles are tested in a liquid-encapsulated environment such as decane, CP, and water, and the influences of the different components and additives on the cohesion can be compared. Surfactants, acids, sorbitan monolaurate (Span20, an anticoagulant), poly-N-vinyl caprolactam (PVCap, a kinetic inhibitor), coatings, and chemically or physically modified surfaces have significant reduction effects on the cohesion and adhesion in a hydrate particle system (Fig. 13) (Aman et al., 2014). Moreover, surfactants and acids change the microscopic morphology of the hydrate shell, which leads to changes in the anti-destruction ability of the hydrate shell (Brown et al., 2016). The adhesion force between CH_4/C_2H_6 mixed gas hydrate particles under the formation environment (2 MPa and −5 °C) is ten times higher than the adhesion between CP(H) in the hydrocarbon-phase environment. Wang et al. (2020) used the MMF apparatus to compare the cohesions of CP(H) and CH_4(H) particles and analyzed the influences of the particle size and setting time on cohesion.

3.2. Adhesion

The force required to pull apart a hydrate particle and a flat plate is defined as the adhesion between the hydrate particle and surface. The adhesion is highly correlated with the surface materials, and lower hydrate adhesion is generally achieved on surfaces with lower free energy. The adhesion between a CP(H) particle and carbon steel (CS) is much lower than the cohesion between CP(H) particles, and it is also lower than the adhesion between an ice particle and CS (Nicholas et al., 2009). In addition, the adhesion is largely influenced by the presence of water. When water droplets are attached to a solid surface (Fig. 14), the adhesion between the hydrate and solid surface is more than 10 times the cohesion between hydrate particles (Aspenes et al., 2010; Cha et al., 2013; Liu

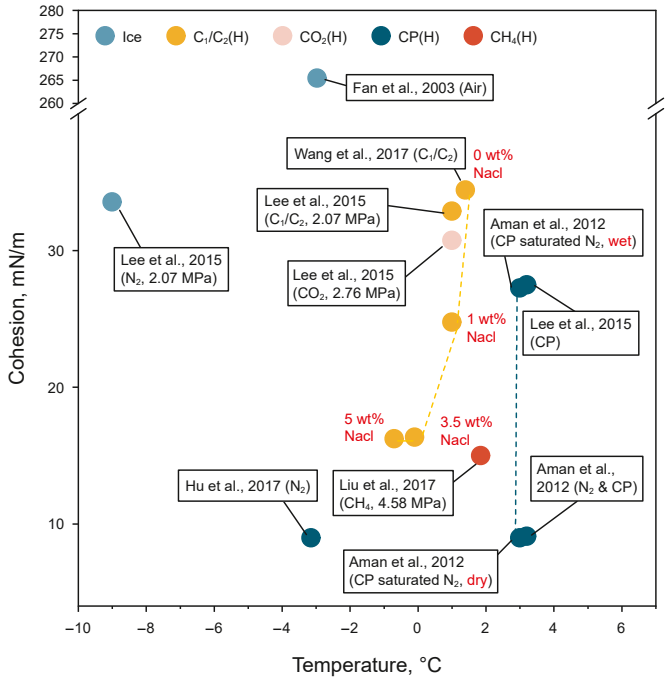

Fig. 12. Measurement results of cohesion (mean value) between different particles in a gas-phase environment.

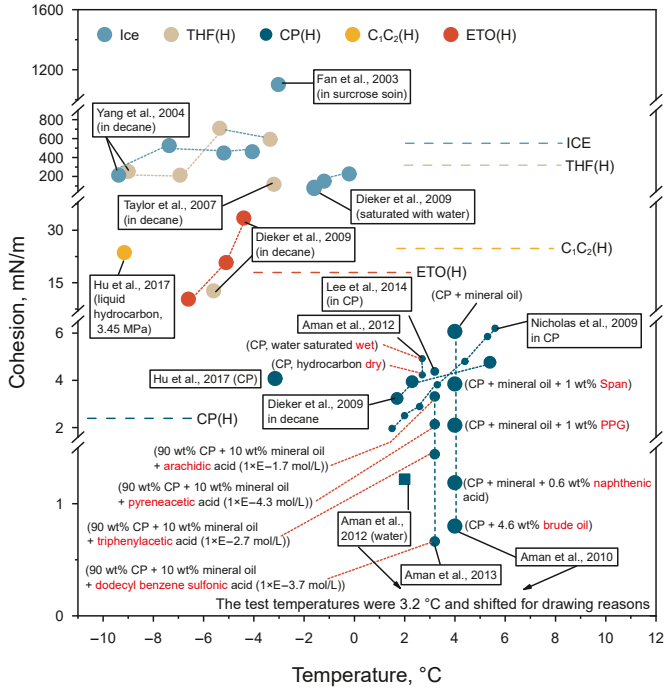

Fig. 13. Cohesion (mean value) measurement results for different particles in liquid-phase environments.

et al., 2015; Song et al., 2010). When the solid surface is wet, the adhesion is the highest, and adding petroleum acid to the oil phase greatly reduces the adhesion (Aspenes et al., 2010). In a high-pressure environment, the surface corrosion caused by the NaCl concentration has a significant impact on the adhesion between a gas hydrate particle and a carbon steel surface (Hu et al., 2017). Liu et al. (2023) found that the liquid bridge is ruptured and rebuilt in

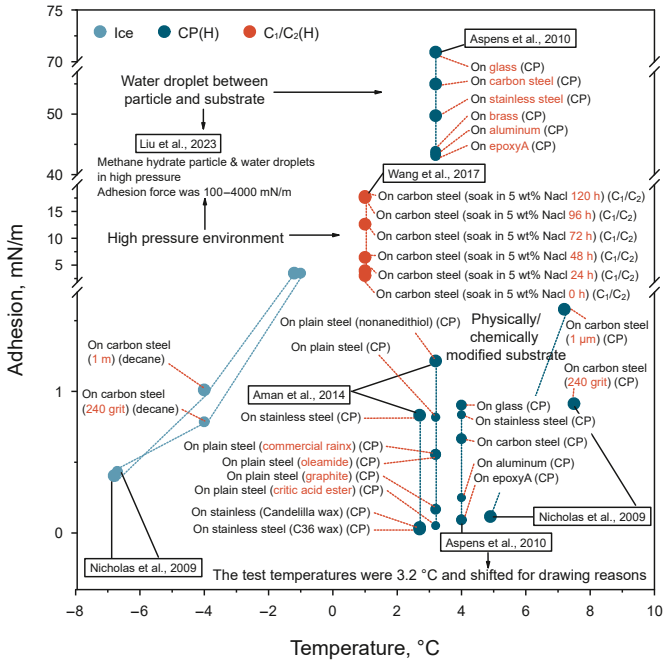

Fig. 14. Test results for adhesion (mean value) between particles and plates under different conditions.

the process of measuring hydrate particles and droplets in a high-pressure gas-phase environment.

3.3. Micro-strength

The abovementioned cohesion and adhesion measurements were carried out between spherical particles and between spherical particles and plates. The contact area was difficult to quantify, so the effective harmonic radius was used to conduct a unified analysis. To obtain an accurate adhesion strength, the experimental methods were improved and the micro-stretching and adhesion tests were carried out under the condition that the contact area was known. As shown in Fig. 15, increasing the contact time and load under gas conditions increased the cohesive strength between CH_4(H) and ice, but the increase in the contact time did not affect the cohesive strength in the water phase. The cohesive strength between CH_4(H) in the water phase was far lower than that in the gas phase. The cohesive strengths of several different types of hydrate particles tested in the gas phase were within a narrow range (Sato et al., 2016).

The adhesion strength of hydrates on surfaces of different materials varies greatly (Fig. 16). Both the surface roughness and hydrate formation time have significant impacts on the adhesion strength (Liu et al., 2020). With increasing surface roughness and hydrate formation time, the adhesion strength increases accordingly. Increasing the undercooling also leads to an increase in the adhesion strength.

The main mechanical test values and conclusions of the above typical hydrate particle system measuring instruments are as follows (Table 2).

4. Mechanical calculation models and theories

Due to the spherical characteristics of hydrate particles, the adhesion between particles can be processed using a spherical particle contact calculation model. However, due to hydrate-phase

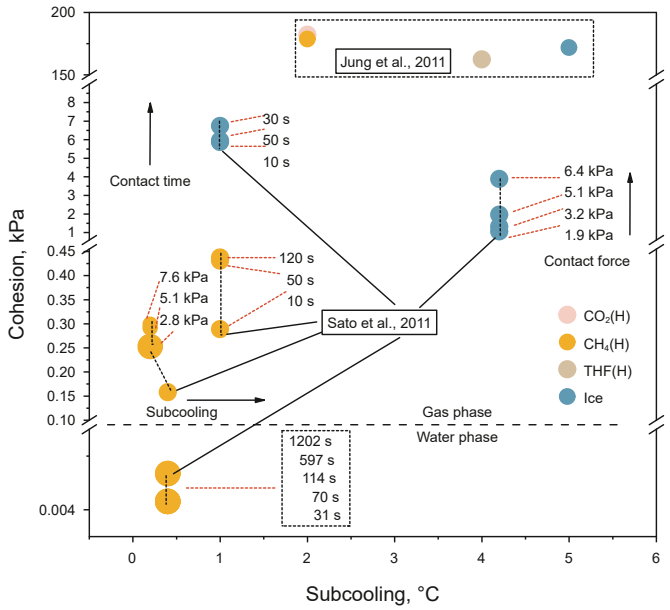

Fig. 15. Measurement results for micro-tensile cohesive strength.

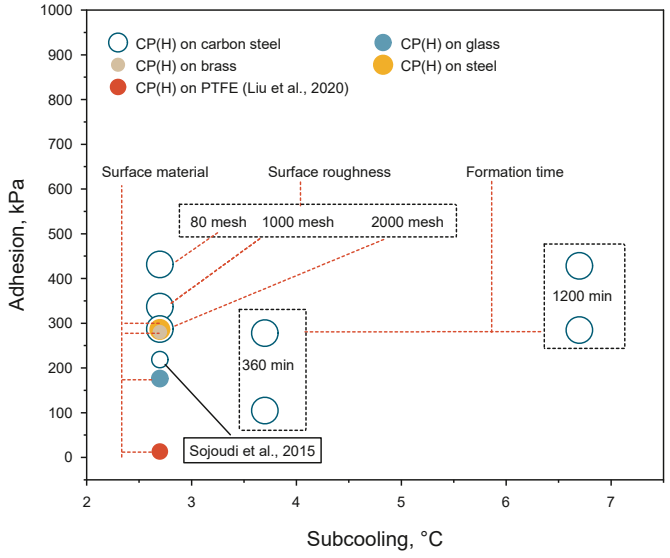

Fig. 16. Measurement results for micro-tensile adhesion (shear) strength.

changes, the frequent solidification of capillary bridges between hydrate particles under high supercooling conditions significantly affects the interaction between hydrate particles (Wu et al., 2020). Some classic spherical particle contact theories and liquid bridge theories are not fully applicable to the calculation of the adhesion between a hydrate particle and a flat plate. The current models for calculating the force between hydrate particles were developed from spherical particles contact liquid bridge model and the hydrate shell model.

4.1. Liquid bridge theory

When two particles with wet surfaces were brought close to each other, one side of the liquid film was gradually fused. Because the surface curvature is large and negative, the liquid on the other side of the film is sucked into the overlapping area, and a stable liquid bridge is formed (Horikawa et al., 2011). Payam et al. (2011) proposed an analytical method for calculating the spherical/spherical geometric capillary force based on the energy principle method. Their method considers spheres with equal radii and non-equal radii, as well as symmetric and asymmetric configurations of the liquid/solid interface. Dörmann et al. (2015) proposed a numerical method for determining the shape of a capillary bridge between spherical particles and calculated its forces. They discussed the relationships between the particle size, relative humidity, and contact angle and concluded that the performance between nanoparticles and microparticles was different. Wang et al. (2016) explored the capillary bridges and capillary forces of two types of axisymmetric power-law particles in a medium equal volume liquid. Their results revealed that the power-law exponent has a significant effect on the capillary force between two power-law particles. Wang et al. (2017a) adopted the energy minimization method to solve the problem numerically and studied the adhesion and fracture behaviors of a capillary liquid bridge between three spheres in an equilibrium state. They measured the hydraulic bridge force through a newly developed apparatus and verified the validity of the numerical solution.

At present, the variables of liquid bridge volume, fluid flow, interfacial tension, humidity, relative distance of particles, particle diameter, contact angle, etc, have been fully studied in the previous work. The numerical and experimental work mentioned above can be referred for when two hydrate particles contact and the liquid bridge does not consolidate.

4.2. Hydrate shell model

The hydrate shell model was proposed by Taylor et al. (2007) for hydrate growth on water droplets entrained in the oil phase (Brown et al., 2016) (Fig. 17). Hydrate nucleation occurred at the water–oil or water–gas interface, and then the thin hydrate shell grew rapidly. As the hydrate grew, the hydrate shell gradually thickened, and finally the water droplet was completely converted into a hydrate particle. The diameters of emulsified water droplets in crude oil pipelines are generally 1–250 μm, with an average diameter of 20–80 μm (Greaves et al., 2008), which depends on the nature of oil and the shear force during mixing. The particle size distribution is highly dependent on the presence of a surfactant in the fluid. The smaller particles are quickly converted into hydrates, while the larger particles remain unconverted inside the liquid for a long period of time. Under hydrate formation conditions, larger water droplets initially have a thin hydrate shell (i.e., 20–50 μm) with liquid water inside and are gradually converted into hydrate particles (Brown et al., 2016). The nature of the hydrate shell is very important for determining the degree of agglomeration, deposition, and exfoliation events. Since the particles contain unconverted water, the rupture of the hydrate shell caused by a compression or shear force is accompanied by the release of water, resulting in extremely high cohesion. In addition, the unconverted water may be quickly converted into hydrate because of the additional nucleation sites generated by the rupture of the shell.

4.3. Mechanical model between hydrate particles, including capillary force and consolidation

Based on the theory of hydrate shell formation, Aman et al. (2010) explained the interaction between CP(H) particles under normal pressure as a function of the contact time, preload, and temperature and proposed a mechanical model between hydrate particles, including the capillary force and consolidation (Fig. 18(a) and (b)). This model predicts the effect of temperature on the cohesion of hydrate particles (Aman et al., 2011). In Eqs. (1)–(3), F_{IP}

Table 2
List of main mechanical test values and conclusions.

Test project			Liquid phase (including oil and water phases)		Gas phase	
Micro-force	Cohesion	Min	0.65 mN/m	90 wt% CP+10 wt% mineral oil + dodecyl benzene sulfonic acid (1*E−3.7 mol/L) (Aman et al., 2013)	8.9 mN/m	N_2&CP (Aman et al., 2012)
		Max	22.8 mN/m	Liquid hydrocarbon, 3.45 MPa (Hu et al., 2017)	34.6 mN/m	C_1/C_2 (Wang et al., 2017a)
	Adhesion	Min	0.03 mN/m	On stainless steel (C36 wax) (CP) (Aman et al., 2014)	3.02 mN/m	On carbon steel (soak in 5 wt% Nacl 0 h)(C_1/C_2) (Wang et al., 2017a)
		Max	3.3 mN/m	On carbon steel (1 mm) (decane) (Nicholas et al., 2009)	17.8 mN/m	On carbon steel (soak in 5 wt% Nacl 120 h) (C_1/C_2) (Wang et al., 2017a)
Micro-strength	Tensile	Min	0.004 kPa	Contact time 31 s, water phase (Sato et al., 2011)	0.16 kPa	Subcooling (0.4°C) (Sato et al., 2011)
		Max	0.005 kPa	Contact time 1202 s, water phase (Sato et al., 2011)	182.19 kPa	CO_2(H) (Jung et al., 2011)
	Shear	Min	There is no relevant literature report		12.75 kPa	CP(H) on PTFE (Liu et al., 2020)
		Max	There is no relevant literature report		430.87 kPa	CP(H) on carbon steel 80 mesh (Liu et al., 2020)

Main conclusion.
1) The cohesion between hydrate particles in the gas phase is twice that in the oil phase and six times that in the water phase (Aman et al., 2012a,b).
2) The cohesion between hydrate particles in the gas phase is linearly related to the effective radius of the particles, but it is unrelated to the particle size in the oil phase and water phase (Wang et al., 2020).
3) Surfactants, acids, anticoagulant, kinetic inhibitor, coatings, and chemically or physically modified surfaces have significant reduction effects on the cohesion and adhesion in a hydrate particle system (Aman et al., 2014).
4) When water droplets are attached to a solid surface, the adhesion between the hydrate and solid surface is more than 10 times the cohesion between hydrate particles (Aspenes et al., 2010; Cha et al., 2013; Liu et al., 2015; Song et al., 2010).
5) Increase in the contact time did not affect the cohesive strength in the water phase. The cohesive strength between CH_4(H) in the water phase was far lower than that in the gas phase (Sato et al., 2016).

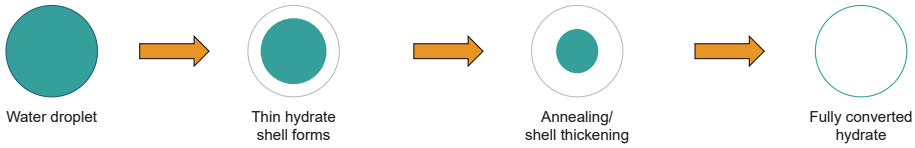

Fig. 17. Proposed mechanism of hydrate formation for a large emulsified water droplet in oil (modified according to Taylor et al. (2007)).

is the force value between particles, γ is the interfacial tension between the liquid bridge and the solid, θ_P is the contact angle, R^* is the effective radius, α is the hug angle, θ_S is the external contact angle, H is the separation distance of the particles, d is the immersion depth of the liquid bridge, τ_t is the tensile strength of the hydrate, χ is the radius of the contact area, and t is the contact time (Aman et al., 2011).

$$F_{IP}=\begin{cases}\dfrac{2\pi\gamma\cos(\theta_P)R^*}{1+\dfrac{H}{2d}}+\pi\gamma\sin(\alpha)\sin(\theta_P+\theta_S)R^* & t\le 30\text{ s}\\ \tau_t\left(\pi\chi^2\right) & t\ge 30\text{ s}\end{cases}. \quad (1)$$

$$R^*=\frac{2R_1R_2}{R_1+R_2}. \quad (2)$$

$$\chi=1.2147\cdot t^{0.1249}. \quad (3)$$

4.4. Modified mechanical model of hydrate particles

However, under high supercooling conditions, the frequent coagulation of the capillary liquid bridges between hydrate particles results in a decrease in the number of liquid bridges, which has a significant impact on the hydrate interaction. The above-mentioned classic mechanical models between hydrate particles, including the capillary force and coagulation, are not suitable for this unique situation. Based on the hydrate shell theory, Liu et al. (2020) established a modified model for calculating the interactions between hydrate shells and considering capillary bridge solidification. They verified the model using measurement results from a newly developed micromechanical dynamometer. Under the condition of low subcooling, the solidification of the capillary bridge is negligible (Liu et al., 2020). The liquid bridge and liquid bridge consolidation models described in the previous section successfully describe hydrate particle–droplet interaction behaviors. However, under the condition of high subcooling, the rapid solidification of the liquid bridge has a significant impact on the interaction behaviors (such as the bridge profile and adhesion) (Cha et al., 2013; Liu et al., 2017; Liu et al., 2015, 2016, 2017, 2017; Song et al., 2010). The authors also found that the formed hydrate particles and the high driving force (i.e., low temperature) cause the liquid bridge to grow and consolidate toward the middle of the liquid bridge at the three-phase contact (TPC) line of the hydrate particles (Liu et al., 2017b). The results also suggest that the rapid solidification decreases the initial contact area and weakens the bonding force between the particle and liquid bridge. In this case, the liquid bridge is composed of two parts: (1) the coating part in contact with the hydrate shell and (2) the body part composed of the pure liquid bridge (Fig. 19). The model can accurately predict the liquid bridge profile and rupture distance in this case. The outline of the liquid bridge at $t+dt$ can be approximated by Eq. (4). The liquid bridge rupture distance can be calculated according to Eq. (5). Where R_{l1} and R_{l2} are the equivalent radii of the droplet on the particle. T_{l1} and T_{l2} are the maximum cap heights of a droplet on a particle. First, the liquid volume distribution among hydrate particles is obtained, and then R_{l1}, R_{l2}, T_{l1} and T_{l2} are calculated (Liu et al., 2017).

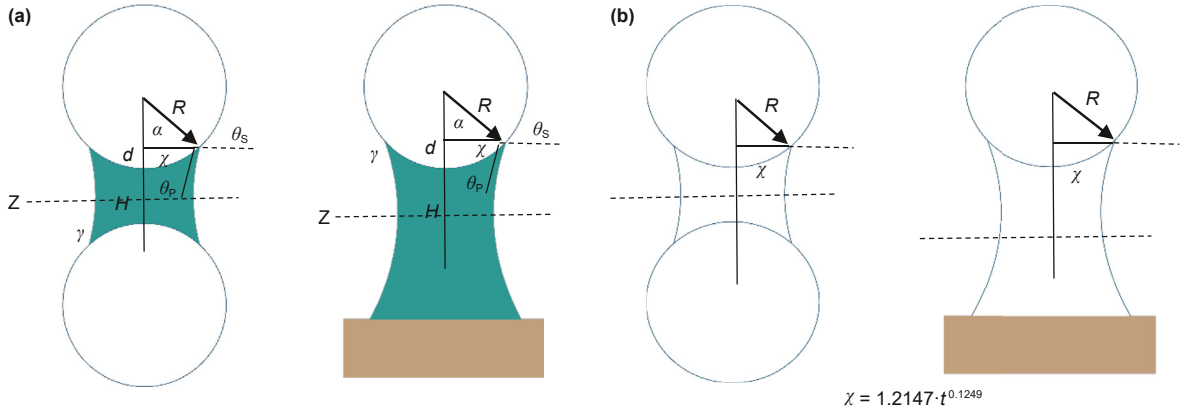

Fig. 18. Sketch of mechanical model between hydrate particles, including capillary force and consolidation: **(a)** Interaction with liquid bridge; **(b)** liquid bridge sintering (adapted from Aman et al. (2011, 2014)).

$$\begin{cases} y(x)_{t+dt|x=0} = a(t)\cdot\Delta x^2 + b(t)\cdot\Delta x + c(t) \\ \pi\int_0^{d_{t+dt}} y(x)_{t+dt}{}^2\cdot\mathrm{d}x = \pi\int_{\Delta x_1}^{d_t-\Delta x_2} y(x)_t{}^2\cdot\mathrm{d}x \\ y(x)_{t+dt|x=d_{t+dt}} = a(t)\cdot(d_t-\Delta x_2)^2 + b(t)\cdot(d_t-\Delta x_2) + c(t) \end{cases} \tag{4}$$

$$2\pi\int_{x=0}^{x=d_t} y(x)_t\sqrt{1+y(x)'_t{}^2}\cdot\mathrm{d}x = 2\pi(R_{11}T_{11}+R_{12}T_{12}) \tag{5}$$

The abovementioned models were developed based on the classic spherical particle contact theory model and the capillary liquid bridge theory and consider the solidification of liquid bridges. These models play an important role in the analysis and calculation of the cohesion/adhesion in hydrate particle systems. However, the state of the liquid bridge during hydrate contact is complicated in the gas phase environment. In addition to unconsolidated and complete consolidation, the liquid bridge will also have weak consolidation state including creep characteristics. This situation should be taken into account in future work.

5. Conclusions and implications

Currently, most studies on the mechanical properties of hydrate-baring sediments have focused on the macro-scale. However, the size of the hydrates between the pores of the sediment particles in actual reservoirs is smaller, especially the dispersed hydrates with a high shale content in the Shenhu area in the South China Sea. Hydrates grow in the pores of sediments, along the surfaces of sediment particles, or in suspended pore fluids, forming various distribution patterns, including pore filling, contact cementation, particle encapsulation, and framework-supported sediments. The contact relationship and mechanical behavior of hydrate particles at the micro-scale directly affect the shear strength and instability behavior of reservoirs. Thus, research on the contact mechanics of hydrate particles at the micro-scale is of great importance.

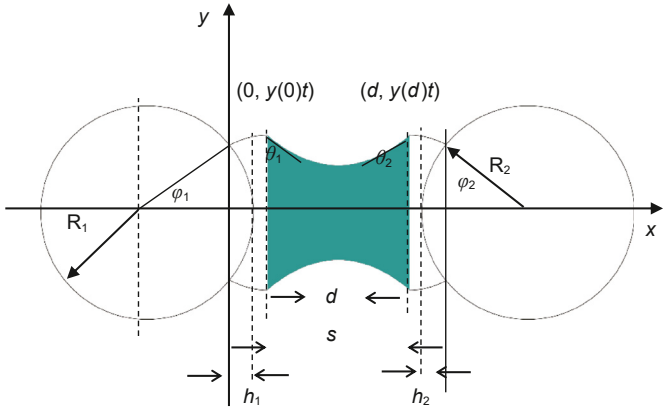

Fig. 19. Sketch of modified mechanical model of hydrate particles (adapted from Liu et al. (2017)).

When the characteristic length of the material is on the micro- or nano-scale, a strong scale effect will occur and will cause the performance of the microscopic material to be significantly different from those of macroscopic materials. The main methods applied in testing the mechanical performances of hydrate particle systems are the cantilever beam method and the micro-stretching method. Among these methods, the micro-stretching method is the most effective method for directly obtaining the mechanical properties of hydrates. However, many difficulties remain in sample centering, clamping, strain measurement, sample fixation, and sample preparation when adopting the micro-stretching method for measuring micron-size hydrate particles. Moreover, even if the micro-structure materials have the same composition and size, different preparation methods will still cause significant differences in their properties. Therefore, how to explain the differences in the basic mechanical properties of these micro-scale structured materials is also a problem that needs to be solved.

Existing hydrate particle contact mechanical tests focus on measuring the normal contact force, the test results of which mainly take into account the influence of liquid bridges between particles or between particles and plates, as well as the effects of liquid bridge solidification. These micromechanical studies have made massive achievements in understanding hydrate formation and blockage in oil and gas transportation pipelines and have provided suggestions for flow assurance. By adding substances such as depressants, anti-polymerization agents, and pipe wall coatings, the adhesion values between hydrate particles and between hydrate particles and pipe walls can be reduced, thereby reducing the accumulation and clogging of hydrate particles in pipelines. However, few measurements have been carried out in the gas phase, especially in environments where methane gas is the main component with agglomerated and clogged hydrate particles. In addition, limited tests in reservoir particles have been conducted in hydrate reservoir exploitation. Micro-force measurements for hydrate particles and

sand particles under simulated actual reservoir environment conditions and high pressure in the water phase also require more development. All of the abovementioned mechanical investigations, as well as particle-scale shear tests conducted to evaluate the instability and sand production of hydrate reservoirs, require more attention to promote our understanding of hydrate mechanics.

With the increasing operation of hydrate trial production in various countries, the sand production caused by the decomposition of hydrates during the depressurization mining process imposes higher requirements for the accurate description of reservoir behaviors. As a result, studying the structure and mechanical properties of hydrate reservoirs from a microscopic perspective will provide a theoretical understanding of reservoir stability and sand control during the test production of hydrates. In future research, micromechanical tests on hydrates will be developed from the measurement of the normal adhesion to the measurement of the tangential friction and shear, and the two measurements will be combined in the test. In particular, the effects of temperature and pressure should be considered. The test results can compare with the existing porothermoelastic wellbore stability model (Cheng et al., 2019). At the same time, the micro-force test will be combined with discrete element numerical simulation (DEM) (Dou et al., 2023). By building an environment close to the real reservoir, some parameters required by DEM will be directly tested at the particle scale. Then the complete set of DEM parameters will be obtained, which reduces the calibration process and increases the accuracy of simulation. In addition, with the continuous development and improvement of modern testing technology, more testing techniques will be integrated into hydrate research and will provide diversified and microscopic solutions for the fundamental research of hydrates. For example, various methods can be applied to nanotribological experiments, such as nanoindentation, scanning tunneling microscopy (STM), scanning electron microscopy (SEM), and friction force microscopy (FFM). The application of these testing methods in hydrate research will promote hydrate investigation. The abovementioned techniques will provide insights into topics that have not been investigated and discovered in current hydrate research.

The formation and stabilization of gas hydrates require relatively harsh conditions, resulting in difficulty in accurately determining hydrate mechanics at small scales, low data accuracy, and unclear surface characteristics and deformation mechanisms of hydrates. Therefore, it is necessary to adopt new research methods and perspectives to conduct a systematic study of the surface characteristics and micromechanical behaviors of gas hydrates at the microscopic scale. From a microscopic perspective, researchers have explored the influences of temperature, pressure, guest molecules, load, contact time, and other factors on the mechanical properties and surface properties of gas hydrates, which have been used to reveal the mechanical properties of hydrate-bearing sediments and the mechanism of hydrate accumulation in pipelines. These studies will help to overcome the fundamental barriers of wellbore stability and formation deformation assessment, prevent hydrate-induced seabed geological disasters, and facilitate the achievement of regional hydrate resource environmental assessment in hydrate exploration and development in the future. In addition, these studies will make practical contributions to the safe and efficient exploration of the hydrate resources in the South China Sea in the future.

CRediT authorship contribution statement

Qiang Luo: Writing – original draft, Investigation, Formal analysis, Data curation. **Wei Li:** Data curation. **Zhi-Hui Liu:** Investigation. **Feng Wang:** Writing – review & editing. **Zhi-Chao Liu:** Writing – review & editing, Conceptualization. **Fu-Long Ning:** Writing – review & editing, Supervision, Conceptualization.

Declaration of competing interest

The authors declare that they have no known competing financial interests or personal relationships that could have appeared to influence the work reported in this paper.

Acknowledgments

This work has been supported by the National Key Research and Development Project (No. 2018YFE0126400), Key Program of Marine Economy Development (Six Marine Industries) Special Foundation of Department of Natural Resources of Guangdong Province (GDNRC [2020]047). We thank LetPub (www.letpub.com) for its linguistic assistance during the preparation of this manuscript.

References

Alberto, M.G., 2021. An experimental description of the double positive effect of CO_2 injection in methane hydrate deposits in terms of climate change mitigation. Chem. Eng. Sci. 233, 116430–116441. https://doi.org/10.1016/j.ces.2020.116430.

Aman, Z.M., Brown, E.P., Sloan, E.D., et al., 2011. Interfacial mechanisms governing cyclopentane clathrate hydrate adhesion/cohesion. Phys. Chem. Chem. Phys. 13, 19796–19806. https://doi.org/10.1039/c1cp21907c.

Aman, Z.M., Dieker, L.E., Aspenes, G., et al., 2010. Influence of model oil with surfactants and amphiphilic polymers on cyclopentane hydrate adhesion forces. Energy & Fuels 24, 5441–5445. https://doi.org/10.1021/ef100762r.

Aman, Z.M., Joshi, S.E., Sloan, E.D., et al., 2012a. Micromechanical cohesion force measurements to determine cyclopentane hydrate interfacial properties. J. Colloid Interface Sci. 376, 283–288. https://doi.org/10.1016/j.jcis.2012.03.019.

Aman, Z.M., Olcott, K., Pfeiffer, K., et al., 2013. Surfactant adsorption and interfacial tension investigations on cyclopentane hydrate. Langmuir 29, 2676–2682. https://doi.org/10.1021/la3048714.

Aman, Z.M., Sloan, E.D., Sum, A.K., et al., 2012b. Lowering of clathrate hydrate cohesive forces by surface active carboxylic acids. Energy & Fuels 26, 5102–5108. https://doi.org/10.1021/ef300707u.

Aman, Z.M., Sloan, E.D., Sum, A.K., et al., 2014. Adhesion force interactions between cyclopentane hydrate and physically and chemically modified surfaces. Phys. Chem. Chem. Phys. 16, 25121–25128. https://doi.org/10.1039/c4cp02927e.

Aspenes, G., Dieker, L.E., Aman, Z.M., et al., 2010. Adhesion force between cyclopentane hydrates and solid surface materials. J. Colloid Interface Sci. 343, 529–536. https://doi.org/10.1016/j.jcis.2009.11.071.

Brown, E.P., Koh, C.A., 2016. Micromechanical measurements of the effect of surfactants on cyclopentane hydrate shell properties. Phys. Chem. Chem. Phys. 18, 594–600. https://doi.org/10.1039/c5cp06071k.

Cha, M., Couzis, A., Lee, J.W., 2013. Macroscopic investigation of water volume effects on interfacial dynamic behaviors between clathrate hydrate and water. Langmuir 29, 5793–5800. https://doi.org/10.1021/la4005664.

Cha, M., Shin, K., Lee, H., et al., 2015. Kinetics of methane hydrate replacement with carbon dioxide and nitrogen gas mixture using in situ NMR spectroscopy. Environ. Sci. Technol. 49, 1964–1971. https://doi.org/10.1021/es504888n.

Chen, X.Y., Yang, J., Gao, D.L., et al., 2020. Unlocking the deepwater natural gas hydrate's commercial potential with extended reach wells from shallow water: Review and an innovative method. Renew. Sustain. Energy Rev. 134, 110388–110408. https://doi.org/10.1016/j.rser.2020.110388.

Cheng, W., Ning, F.L., Sun, J.X., et al., 2019. A porothermoelastic wellbore stability model for riserless drilling through gas hydrate-bearing sediments in the Shenhu area of the South China Sea. J. Nat. Gas Sci. Eng. 72, 103036–103049. https://doi.org/10.1016/j.jngse.2019.103036.

Collett, T., Bahk, J.J., Baker, R., et al., 2014. Methane hydrates in nature—Current knowledge and challenges. J. Chem. Eng. Data 60, 319–329. https://doi.org/10.1021/je500604h.

Dieker, L.E., Aman, Z.M., George, N.C., et al., 2009. Micromechanical adhesion force measurements between hydrate particles in hydrocarbon oils and their modifications. Energy & Fuels 23, 5966–5971. https://doi.org/10.1021/ef9006615.

Dörmann, M., Schmid, H.J., 2015. Simulation of capillary bridges between particles. Procedia Eng. 102, 14–23. https://doi.org/10.1016/j.proeng.2015.01.102.

Dou, X.F., Liu, Z.C., Ning, F.L., et al., 2023. 3D DEM modeling on mechanical weakening of gas hydrate-bearing sandy sediments during hydrate dissociation. Comput. Geotech. 154, 105116–105133. https://doi.org/10.1016/j.compgeo.2022.105116.

Durham, W.B., Kirby, S.H., Stern, L.A., et al., 2003. The strength and rheology of methane clathrate hydrate. J. Geophys. Res. Solid Earth 108, 2–11. https://doi.org/10.1029/2002jb001872.

Fan, X., Ten, P., Clarke, C., et al., 2003. Direct measurement of the adhesive force between ice particles by micromanipulation. Powder Technol. 131, 105–110. https://doi.org/10.1016/s0032-5910(02)00339-x.

Greaves, D., Boxall, J., Mulligan, J., et al., 2008. Hydrate formation from high water content-crude oil emulsions. Chem. Eng. Sci. 63, 4570–4579. https://doi.org/10.1016/j.ces.2008.06.025.
Guo, D.D., Ou, W.J., Ning, F.L., et al., 2020. The effects of hydrate formation and dissociation on the water-oil interface: insight into the stability of an emulsion. Fuel 266, 116980–116991. https://doi.org/10.1016/j.fuel.2019.116980.
Hammerschmidt, E.G., 1934. Formation of gas hydrates in natural gas transmission lines. Ind. Eng. Chem. 26, 851–855. https://doi.org/10.1021/ie50296a010.
Horikawa, T., Do, D.D., Nicholson, D., 2011. Capillary condensation of adsorbates in porous materials. Adv. Colloid Interface Sci. 169, 40–58. https://doi.org/10.1016/j.cis.2011.08.003.
Hu, S.J., Koh, C.A., 2017. Interfacial properties and mechanisms dominating gas hydrate cohesion and adhesion in liquid and vapor hydrocarbon phases. Langmuir 33, 11299–11309. https://doi.org/10.1021/acs.langmuir.7b02676.
Hyodo, M., Li, Y., Yoneda, J., et al., 2013. Mechanical behavior of gas-saturated methane hydrate-bearing sediments. J. Geophys. Res. Solid Earth 118, 5185–5194. https://doi.org/10.1002/2013jb010233.
Jin, S., Nagao, J., Takeya, S., et al., 2006. Structural investigation of methane hydrate sediments by microfocus X-ray computed tomography technique under high-pressure conditions. Jpn. J. Appl. Phys. 45, L714–L716. https://doi.org/10.1143/jjap.45.L714.
Jung, J.W., Santamarina, J.C., 2011. Hydrate adhesive and tensile strengths. G-cubed 12, 1–9. https://doi.org/10.1029/2010gc003495.
Koh, C.A., Sloan, E.D., Sum, A.K., et al., 2011. Fundamentals and applications of gas hydrates. Annu. Rev. Chem. Biomol. Eng. 2, 237–257. https://doi.org/10.1146/annurev-chembioeng-061010-114152.
Lee, B.R., Koh, C.A., Sum, A.K., 2014. Development of a high pressure micromechanical force apparatus. Rev. Sci. Instrum. 85, 95120–95124. https://doi.org/10.1063/1.4896661.
Lee, B.R., Sa, J.-H., Park, D.-H., et al., 2011. “Continuous” method for the fast screening of thermodynamic promoters of gas hydrates using a quartz crystal microbalance. Energy & Fuels 26, 767–772. https://doi.org/10.1021/ef201414u.
Lee, B.R., Sum, A.K., 2015. Micromechanical cohesion force between gas hydrate particles measured under high pressure and low temperature conditions. Langmuir 31, 3884–3888. https://doi.org/10.1021/acs.langmuir.5b00361.
Li, W., Fang, B., Tao, Z.T., et al., 2024. Probing the instability of surface structure on solid Hydrates: a microscopic perspective through experiment and simulation. Appl. Surf. Sci. 648, 158971–158985. https://doi.org/10.1016/j.apsusc.2023.158971.
Li, W., Pang, J.T., Peng, L., et al., 2023. Microscopic insights into the effects of anti-agglomerant surfactants on surface characteristics of tetrahydrofuran hydrate. Energy & Fuels 37, 3741–3751. https://doi.org/10.1021/acs.energyfuels.2c04254.
Li, X.S., Xu, C.G., Zhang, Y., et al., 2016. Investigation into gas production from natural gas hydrate: A review. Appl. Energy 172, 286–322. https://doi.org/10.1016/j.apenergy.2016.03.101.
Liu, C.W., Li, M.Z., Chen, L.T., et al., 2017a. Experimental investigation on the interaction forces between clathrate hydrate particles in the presence of a water bridge. Energy & Fuels 31, 4981–4988. https://doi.org/10.1021/acs.energyfuels.7b00364.
Liu, C.W., Li, M.Z., Liu, C.T., et al., 2016. Micromechanical interactions between clathrate hydrate particles and water droplets: experiment and modeling. Energy & Fuels 30, 6240–6248. https://doi.org/10.1021/acs.energyfuels.6b00668.
Liu, C.W., Li, M.Z., Zhang, G.D., et al., 2015. Direct measurements of the interactions between clathrate hydrate particles and water droplets. Phys. Chem. Chem. Phys. 17, 20021–20029. https://doi.org/10.1039/c5cp02247a.
Liu, C.W., Li, Y.X., Wang, W.Y., et al., 2017b. Modeling the micromechanical interactions between clathrate hydrate particles and water droplets with reducing liquid volume. Chem. Eng. Sci. 163, 44–55. https://doi.org/10.1016/j.ces.2017.01.031.
Liu, C.W., Wang, Z.Y., Tian, J.L., et al., 2020a. Fundamental investigation of the adhesion strength between cyclopentane hydrate deposition and solid surface materials. Chem. Eng. Sci. 217, 115524–115533. https://doi.org/10.1016/j.ces.2020.115524.
Liu, C.W., Zhang, C.R., Zhou, C.R., et al., 2020b. Effects of the solidification of capillary bridges on the interaction forces between hydrate particles. Energy & Fuels 34, 4525–4533. https://doi.org/10.1021/acs.energyfuels.0c00463.
Liu, C.W., Zhou, C.R., Li, M.Z., et al., 2023. Direct measurements of the interactions between methane hydrate particle-particle/droplet in high pressure gas phase. Fuel 332, 12619001. https://doi.org/10.1016/j.fuel.2022.126190, 11269009.
Liu, R., Wang, H., Li, X., et al., 2008. A micro-tensile method for measuring mechanical properties of MEMS materials. J. Micromech. Microeng. 18, 6500201–6500207. https://doi.org/10.1088/0960-1317/18/6/065002.
Liu, Z.C., Ning, F.L., Hu, G.W., et al., 2020c. Characterization of seismic wave velocity and attenuation and interpretation of tetrahydrofuran hydrate-bearing sand using resonant column testing. Mar. Petrol. Geol. 122, 104620–104630. https://doi.org/10.1016/j.marpetgeo.2020.104620.
Liu, Z.C., Wei, H.Z., Peng, L., et al., 2017. An easy and efficient way to evaluate mechanical properties of gas hydrate-bearing sediments: the direct shear test. J. Petrol. Sci. Eng. 149, 56–64. https://doi.org/10.1016/j.petrol.2016.09.040.
Luo, Q., Liu, Z.H., Ning, F.L., et al., 2022. Micromechanical tangential force measurements between tetrahydrofuran hydrate particles. Fuel 316, 12307301–12307308. https://doi.org/10.1016/j.fuel.2021.123073.
Miyazaki, K., Masui, A., Sakamoto, Y., et al., 2011. Triaxial compressive properties of artificial methane-hydrate-bearing sediment. J. Geophys. Res. 116. https://doi.org/10.1029/2010jb008049. B0610201-B0610211.
Nguyen, N.N., Berger, R., Kappl, M., et al., 2021. Clathrate adhesion induced by quasi-liquid layer. J. Phys. Chem. C. Nanomater Interfaces 125, 21293–21300. https://doi.org/10.1021/acs.jpcc.1c06997.
Nicholas, J.W., Dieker, L.E., Sloan, E.D., et al., 2009. Assessing the feasibility of hydrate deposition on pipeline walls-adhesion force measurements of clathrate hydrate particles on carbon steel. J. Colloid Interface Sci. 331, 322–328. https://doi.org/10.1016/j.jcis.2008.11.070.
Ning, F.L., Yu, Y.B., Kjelstrup, S., et al., 2012. Mechanical properties of clathrate hydrates: status and perspectives. Energy Environ. Sci. 5, 6779–6795. https://doi.org/10.1039/c2ee03435b.
Notley, S.M., Eriksson, M., Wagberg, L., 2005. Visco-elastic and adhesive properties of adsorbed polyelectrolyte multilayers determined in situ with QCM-D and AFM measurements. J. Colloid Interface Sci. 292, 29–37. https://doi.org/10.1016/j.jcis.2005.05.057.
Ohmura, R., Shigetomi, T., Mori, Y.H., 2002. Bending tests on clathrate hydrate single crystals. Philos. Mag. A 82, 1725–1740. https://doi.org/10.1080/01418610208235686.
Payam, A.F., Fathipour, M., 2011. A capillary force model for interactions between two spheres. Particuology 9, 381–386. https://doi.org/10.1016/j.partic.2010.11.004.
Peng, L., Li, W., Ning, F.L., et al., 2019. Micromechanical tests of tetrahydrofuran hydrate using atomic force microscope. Scientia Sinica Technologica 50, 31–40. https://doi.org/10.1360/sst-2019-0170.
Peng, L., Ning, F.L., Li, W., et al., 2018. Investigation on the effect of growth temperature and contact interface on surface characteristics of THF clathrate hydrates by atomic force microscopy. Scientia Sinica Physica, Mechanica & Astronomica 49. https://doi.org/10.1360/sspma2018-00182, 034612-034621.
Petrenko, V.F., 1997. Study of the surface of ice, ice/solid and ice/liquid interfaces with scanning force microscopy. J. Phys. Chem. B 101, 6276–6281. https://doi.org/10.1021/jp963217h.
Rabinovich, Y.I., Adler, J.J., Esayanur, M.S., et al., 2002. Capillary forces between surfaces with nanoscale roughness. Adv. Colloid Interface Sci. 96, 213–230. https://doi.org/10.1016/s0001-8686(01)00082-3.
Sato, J., Iida, T., Kiyono, F., et al., 2016. Cohesion force measurement of methane hydrate and numerical simulation of rising bubbles covered with a hydrate membrane within a contracting pipe. Energy & Fuels 30, 7100–7107. https://doi.org/10.1021/acs.energyfuels.6b01341.
Schindler, M., Batzle, M.L., Prasad, M., 2017. Micro X-Ray computed tomography imaging and ultrasonic velocity measurements in tetrahydrofuran-hydrate-bearing sediments. Geophys. Prospect. 65, 1025–1036. https://doi.org/10.1111/1365-2478.12449.
Seol, Y., Lei, L., Choi, J.H., et al., 2019. Integration of triaxial testing and pore-scale visualization of methane hydrate bearing sediments. Rev. Sci. Instrum. 90, 12450401–12450407. https://doi.org/10.1063/1.5125445.
Sloan, E.D., 2007. Clathrate Hydrates of Natural Gases. Third Edition.
Sloan, E.D., 2003. Fundamental principles and applications of natural gas hydrates. Nature (London) 426, 353–359. https://doi.org/10.1038/nature02135.
Smith, J.D., Meuler, A.J., Bralower, H.L., et al., 2012. Hydrate-phobic surfaces: fundamental studies in clathrate hydrate adhesion reduction. Phys. Chem. Chem. Phys. 14, 6013–6020. https://doi.org/10.1039/c2cp40581d.
Sojoudi, H., Walsh, M.R., Gleason, K.K., et al., 2015. Investigation into the formation and adhesion of cyclopentane hydrates on mechanically robust vapor-deposited polymeric coatings. Langmuir 31, 6186–6196. https://doi.org/10.1021/acs.langmuir.5b00413.
Song, J.H., Couzis, A., Lee, J.W., 2010a. Direct measurements of contact force between clathrate hydrates and water. Langmuir 26, 9187–9190. https://doi.org/10.1021/la101309j.
Song, J.H., Couzis, A., Lee, J.W., 2010b. Investigation of macroscopic interfacial dynamics between clathrate hydrates and surfactant solutions. Langmuir 26, 18119–18124. https://doi.org/10.1021/la103193m.
Song, Y.C., Yu, F., Li, Y.H., et al., 2010c. Mechanical property of artificial methane hydrate under triaxial compression. J. Nat. Gas Chem. 19, 246–250. https://doi.org/10.1016/s1003-9953(09)60073-6.
Stern, L.A., Kirby, S.H., Circone, S., et al., 2004. Scanning Electron Microscopy investigations of laboratory-grown gas clathrate hydrates formed from melting ice, and comparison to natural hydrates. Am. Mineral. 89, 1162–1175.
Taylor, C.J., Dieker, L.E., Miller, K.T., et al., 2007. Micromechanical adhesion force measurements between tetrahydrofuran hydrate particles. J. Colloid Interface Sci. 306, 255–261. https://doi.org/10.1016/j.jcis.2006.10.078.
Teng, Y., Wang, P., Zhou, Y., et al., 2021. Potential applications of distributed optical fiber sensor in hydrate-induced sedimentary deformation research. Energy Sci. Eng. 10, 4–12. https://doi.org/10.1002/ese3.1016.
Wang, J.-P., Gallo, E., François, B., et al., 2017a. Capillary force and rupture of funicular liquid bridges between three spherical bodies. Powder Technol. 305, 89–98. https://doi.org/10.1016/j.powtec.2016.09.060.
Wang, S.L., Hu, S.J., Brown, E.P., et al., 2017b. High pressure micromechanical force measurements of the effects of surface corrosion and salinity on CH_4/C_2H_6 hydrate particle-surface interactions. Phys. Chem. Chem. Phys. 19, 13307–13315. https://doi.org/10.1039/c7cp01584d.
Wang, D.D., Liu, Z.C., Ning, F.L., et al., 2020a. Dynamic responses of THF hydrate-bearing sediments under small strain: resonance column test. J. Nat. Gas Sci. Eng. 81, 103399–103412. https://doi.org/10.1016/j.jngse.2020.103399.
Wang, L., Su, F., Xu, H., et al., 2016. Capillary bridges and capillary forces between two axisymmetric power–law particles. Particuology 27, 122–127. https://doi.org/10.1016/j.partic.2015.08.005.

Wang, S.L., Fan, S.S., Lang, X.M., et al., 2020b. Particle size dependence of clathrate hydrate particle cohesion in liquid/gaseous hydrocarbons. Fuel 259, 116201–116208. https://doi.org/10.1016/j.fuel.2019.116201.

Winters, W.J., Waite, W.F., Mason, D.H., et al., 2007. Methane gas hydrate effect on sediment acoustic and strength properties. J. Petrol. Sci. Eng. 56, 127–135. https://doi.org/10.1016/j.petrol.2006.02.003.

Wu, P., Li, Y.H., Sun, X., et al., 2020. Mechanical characteristics of hydrate-bearing sediment: A review. Energy Fuel. 35, 1041–1057. https://doi.org/10.1021/acs.energyfuels.0c03995.

Yang, S., Kleehammer, D.M., Huo, Z.X., et al., 2004. Temperature dependence of particle-particle adherence forces in ice and clathrate hydrates. J. Colloid Interface Sci. 277, 335–341. https://doi.org/10.1016/j.jcis.2004.04.049.

Yoneda, J., Masui, A., Konno, Y., et al., 2015. Mechanical properties of hydrate-bearing turbidite reservoir in the first gas production test site of the Eastern Nankai Trough. Mar. Petrol. Geol. 66, 471–486. https://doi.org/10.1016/j.marpetgeo.2015.02.029.

Yu, Y.J., Luo, Q., Ning, F.L., 2021. Direct measurement of the interaction forces between sediment particles in gas hydrate reservoirs. Journal of China University of Petroleum (Edition of Natural Science) 45, 87–93. https://doi.org/10.3969/j.issn.1673-5005.2021.01.001.

Zhang, X.H., Lu, X.B., Shi, Y.H., et al., 2015. Study on the mechanical properties of hydrate-bearing silty clay. Mar. Petrol. Geol. 67, 72–80. https://doi.org/10.1016/j.marpetgeo.2015.04.019.